Chemically Fueled Self-sorted Hydrogels

Nishant Singh,[±]* *Álvaro López-Acosta,*[±] *Georges J.M. Formon, Thomas M. Hermans**

Address: Université de Strasbourg, CNRS, UMR7140, 4 Rue Blaise Pascal, 67081 Strasbourg, France E-mail: nishant.singh@unistra.fr, hermans@unistra.fr

Keywords: chemical fuels, self-sorting, hydrogels, secondary nucleation, multicomponent systems.

Abstract: Narcissistic self-sorting in supramolecular assemblies can help to construct materials with more complex hierarchies. Whereas controlled changes in pH or temperature have been used to this extent for two-component self-sorted gels, here we show that a chemically fueled approach can provide three-component materials with high precision. The latter materials have interesting mechanical properties, such as enhanced or suppressed stiffness, and intricate multi-step gelation kinetics. In addition, we show that we can achieve supramolecular templating, where pre-existing supramolecular fibers first act as a templates for growth of a second gelator, after which they can selectively be removed.

1. Introduction

Narcissistically self-sorted hydrogels have been made by methods like rapid mixing of components,[1] solvent switching,[2] chiral recognition,[3] electrostatic interactions,[4] pH change,[5, 6] and supramolecular catalysis.[5, 6] Thermal annealing is most commonly used, where different gelation temperatures of the molecules allow them to self-assemble sequentially.[7-10] A second approach, uses a gradual change in pH to create two-component self-sorted hydrogels. Gluconolactone (GdL) hydrolysis leads to sequential gelation of co-dissolved monomers at their respective pK_a values, leading to materials with improved mechanical, optoelectronic, and photoconductive properties.[11-19]

van Esch and co-workers have shown fabrication of self-sorted hydrogels using 'kinetic self-sorting' of both a charged and neutral hydrogelator which form *in situ* via hydrazone formation. The reaction kinetics of the hydrogelators were found to be comparable, but they could still self-sort in certain cases due to their differing minimum gelation concentrations.[20]

Here we show that a chemically fueled functional group transformation—that is, aldehyde–to–hydroxysulfonate (and back)—can lead to exquisite control over self-sorting, providing access to well-structured three-component hydrogels. This approach is useful, since chemically very similar gelators with different innate reactivity can be used, which would otherwise co-assemble when using controlled cooling. Moreover, since the functional group transformation is reversible, we can achieve supramolecular templating, where first a self-assembled fiber guides the growth of a second, after which the first can be selectively removed. Overall, we believe chemically fueled approaches are promising to get more exquisite control over supramolecular structure and the mechanical properties of multi-component gels.

2. Results and discussion

We recently reported a chemically fueled reaction cycle capable of gel-sol-gel transitions using aldehyde-containing saccharide derivative (compound **3** in Figure 1a).[21] In the latter, a thermally annealed hydrogel of **3** was first disassembled using sodium dithionite DT by converting the aldehyde moiety into its water-soluble hydroxysulfonate analog **3'**. Formaldehyde (HCHO), produced *in situ* with a time-delay, then converted sulfonate **3'** back to aldehyde **3**, again leading to gelation.

In the current work, we synthesized compounds **1** and **2** with close structural similarity to **3** and studied their assembly behavior in heat–cool cycles and their response to chemical fuels,

both for the pure compounds and that of their mixtures (Figure 1). Surprisingly, this led to up to three-component well-structured self-sorted hydrogels.

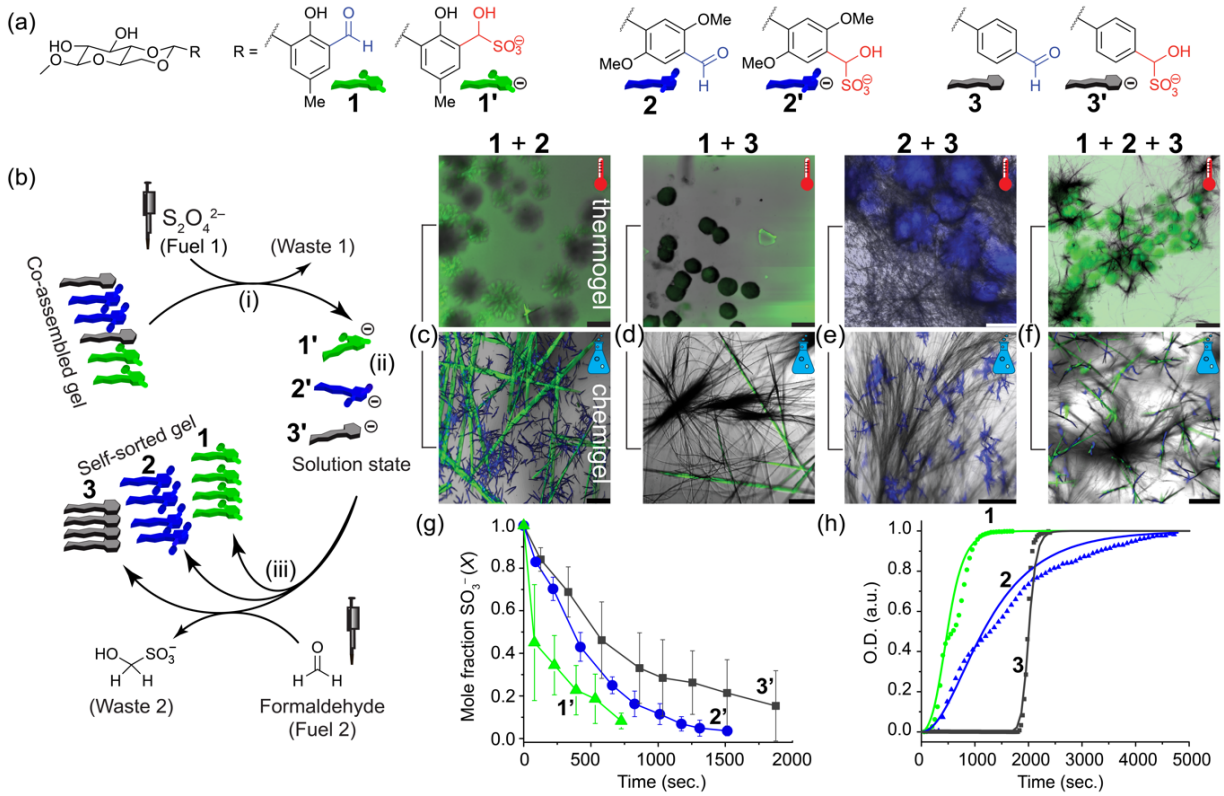

Figure 1: Self-sorting achieved by a chemical fuel. (a) Chemical structures of the used gelators, and their sulfonate analogs (numbers with prime indication). **(b)** Scheme starting from a co-assembled thermogel that is disassembled by fuel 1 (i), resulting in a solution state (ii). After addition of fuel 2 (iii) a self-sorted gel is formed. Confocal images of thermally annealed (top), or chemically fueled (bottom) assemblies: **(c) 1**+**2**, **(d) 1**+**3**, **(e) 2**+**3**, **(f) 1**+**2**+**3**. **(g)** Kinetics of consumption of **1'**, **2'**, and **3'** (21.6 mM) after HCHO (~44 eq.) addition from ^{1}H-NMR. **(h)** Self-assembly kinetics from turbidity measurements at 500 nm using UV-Vis spectroscopy. Points are raw data, solid lines fits to a kinetic model (see main text). Assemblies of **1**, **2**, and **3** (21.6 mM) from **1'**, **2'**, and **3'** upon addition of HCHO (47 eq.).

Thermally annealed 'thermogels'

We started from the traditional 'controlled cooling' approach[7-10] to try and obtain self-sorted hydrogels. Both pure **1** as well as **2** formed free standing hydrogels by thermal annealing with critical gelation concentration (CGC) of 23.5 mM and 21.6 mM, respectively. As a reminder, we had previously shown that thermogel **3** had a CGC of 25.8 mM.[21] Such 'thermogels' have gelation temperatures (T_{gel} at 35 mM) of 74°C for **1**, 78°C for **2**, and 60°C for **3**, as described in SI section S3.1. Confocal laser scanning microscopy (CLSM, including transmitted light imaging) showed that thermogel **1** (35 mM) formed a bimodal distribution of green fluorescent fibers: small fibers of width < 1 μm and length ~ 200 μm, and long fibers of width ~10 μm and length >500 μm. The latter were also much more emissive as compared to the short fibers. Thermogels of **2** showed large ~ 400 μm blue fluorescent spherulites while **3** formed thin (1–2 μm) and long (>1000 μm) non-fluorescent fibers (SI Figure S1a). Next, we tested thermally annealed two- and three-components combinations of these molecules (total concentration is always constant at 35 mM). Thermogel **1**+**2** (ratio 0.5 : 0.5) formed a free-standing hydrogel composed of co-assembled spherules (Figure 1c) with an intermediate emission wavelength λ_{em}= 523 nm, as compared to the pure assemblies that were 548 and 485 nm, respectively. The latter suggests that **1** and **2** co-assemble, when thermally cycled. In addition, the fibrous structure of **1** was completely suppressed in the **1**+**2** gel, further supporting co-assembly. Thermogel **1**+**3** only formed spherical co-assembled aggregates, whereas pure **1** and **3** both form long fibers. The fluorescence emission wavelength is identical to that of **1**, since **3** is non-emissive. In addition, gelation was suppressed, whereas pure **1** and **3** both form gels at 35 mM at room temperature. This shows that co-assembly can be detrimental for heat–cool thermogels. The combination of **2**+**3** formed self-sorted hydrogels, where the characteristic features of pure **2** and **3**—being blue spherulites and non-emissive fibers, respectively (cf. Figure S1)—can be recognized. The latter makes sense, as **3** has a T_{gel} that is 18 degrees lower than that of **2**. Therefore, during cooling from 85°C to room

temperature, first **2** has time to form, followed by **3** later on. The same argumentation, however, does not hold for **1**+**3**, which have gelation temperatures that are 14 degrees apart, but still co-assemble. Three-component mixtures of **1**+**2**+**3** (ratio: 0.2/0.2/0.6 and 0.33/0.33/0.33) showed features of co-assembled spherical **1**+**2**, and some fibrous **3** albeit much shorter than in pure **3**. Overall, multicomponent thermogels were mostly unable to self-sort except for the combination **2**+**3**. Instead, co-assembly was preferred, leading to loss of their fibrillar morphology and in select cases their gel-forming ability.

Chemically fueled 'chemigels'

We now move to chemically fueled gels or 'chemigels' as we will refer to them. Typically, ~6 equivalents of DT were added to a previously formed thermogel, leading to chemical conversion of the aldehyde moiety to a hydroxysulfonate (i.e., **1'**, **2'**, or **3'**), which resulted in complete dissolution. After 21 hours to ensure full disassembly and dissolution, HCHO was added to revert the hydroxysulfonate back to the aldehyde inducing re-assembly.

Looking first at pure chemigels, we see that **1** still forms green emissive fibers as compared to the thermogel. However, they are not bi-modal in size distribution, but instead more uniform and straight. Compound **2** is also still forming spherulites, but they are 20 times smaller (at 20–30 μm) as compared to the thermally annealed case (cf. Figure S2a). The latter indicates that there are more frequent nucleation events when chemically fueled. And lastly, compound **3** forms non-emissive long fibers both in the thermogels and chemigels. Thermally, the fibers are randomly distributed in space (homogeneous nucleation), whereas chemically they grow more from defined nucleation centers into fractal-like structures, due to secondary nucleation as we showed previously.[21]

For multicomponent systems, **1'**, **2'**, and **3'** were mixed when fully disassembled, followed by addition of HCHO to form the multicomponent chemigels. That is, no heating or cooling procedures were involved to make chemigels. Strikingly, all multicomponent chemigels give

rise to self-sorted assemblies (see Figure 1c–f), whereas this was only the case for **2**+**3** thermally. Even the **1**+**2**+**3** chemigel is self-sorted into the three characteristic green/blue/black (non-emissive) colors.

Upon closer inspection, there is another interesting change in the assembly process of **2**. Instead of self-nucleating and forming blue spherulites (cf. Figure S2a), it grows on top of green fibers of compound **1**, if present. That is, secondary nucleation of **2**, using assemblies of **1** as nucleation sites, is more favorable than homogeneous nucleation. The result is that green fibers are formed, which have blue protrusions from its sides (Figure 1c, SI Figure S2b, SI Movie 1 and 2). Compound **2**, however, does not perform a secondary nucleation on top of **3** (see Figure S2b), likely because their chemical structures are too different from each other, favoring full narcissistic self-sorting. Overall, excellent self-sorting behavior is achieved using our chemically fueled (HCHO) approach. To understand why this is the case, we have examined the chemical and self-assembly kinetics of each building block, which is described next.

Chemical reactivity determines the order of formation

The rate at which the individual hydroxysulfonates revert back to their respective aldehydes was determined by time-dependent ^{1}H NMR kinetics (Figure 1g). The rates of hydroxysulfonate consumption were found to be **1'** > **2'** > **3'**, which can be explained by looking at their chemical structures. Namely, compounds **1** and **2** have electron donating groups: **1** has ortho-hydroxyl and meta-methyl substituents, and **2** has two methoxy groups at the ortho and meta positions. This makes negatively charged **1'** and **2'** more unstable causing them to convert into their corresponding aldehydes and assemble faster as compared to **3'**→**3**. The electron donating capacity of these substituents (OH≥OMe>Me)[22] should render **1'** more unstable than **2'**. Moreover, an –OH group next to the –CHO can further stabilize **1** as a product through intra-molecular hydrogen bonding and accelerate hydroxysulfonate to

aldehyde conversion[23-25, 31] (as confirmed by NMR, see SI Figure S8). Thus, the overall rates of reaction **1** > **2** > **3** are in line with their aromatic substitution pattern.

Cooperative supramolecular polymerization for all derivatives

Once **1'**–**3'** has been chemically converted to its aldehyde form **1**–**3**, it is charge neutral and can start assembling. The assembly kinetics were followed by UV-Vis turbidity measurements, where the optical density (O.D.) at 500 nm was tracked after addition of a large excess (~47 equivalents) of HCHO to hydroxysulfonate solutions (Figure 1h).

UV-Vis turbidity measurements elucidated a cooperative mechanism of self-assembly for all three systems (Figure 1, SI Figure S5). Measurements for **1** and **3** fit best to a kinetic model with secondary nucleation where nucleation is followed by fast elongation, and subsequent secondary nucleation process (growth of new fibers from pre-existing structures). The (primary) nucleation–elongation model gave best fit for data of **2**. Corresponding to the rate of hydroxysulfonate consumption by NMR studies, the rate of self-assembly obtained by UV-Vis measurements and kinetic fitting gave the order of assembly as **1** > **2** > **3** (Figure 1, SI Figure S5, and section 3.6 of SI). Overall, **1** aggregates faster, followed by **2**, and **3** has the slowest polymerization kinetics. This is evidenced by a rate constant for primary nucleation (k_n) 10 orders of magnitude smaller for **3** when compared to **1** and **2** (which have values in the same order of magnitude). After nucleation, aggregates of **1** grow faster than **2** due to a ~2.3 times higher elongation rate constant (k_p) and the presence of secondary nucleation that is not observed in the aggregation of **2** and is only important after nucleation. Confocal images and videos further confirmed this order of assembly in multicomponent mixtures forming self-sorted structures (Figure 1, SI Figure S3, SI Movie 1, 2, 3).

Selective supramolecular template removal

As shown above in Figure 1c, compound **2** can grow on top of assemblies of compound **1** due to secondary nucleation, leading to **1**+**2** structures. Interestingly, we found that upon addition of DT to **1**+**2** structures, we could selectively remove **1** (see disappearance of green **1** fibers in Figure 2a; see also SI Figure S4, SI Movie 4). Considering their reactivity—where the rate of **1'→1** was faster than **2'→2** (Figure 1g)—we had expected that **2→2'** would be faster than **1→1'**. That is, the electron donating groups (OH>OMe>Me) would render **2'** more stable than **1'**, and therefore **2** should react faster with DT as compared to **1**. However, the reverse is observed, and **1** that forms first upon addition of HCHO (see Figure S4b), also disappears first when adding DT.

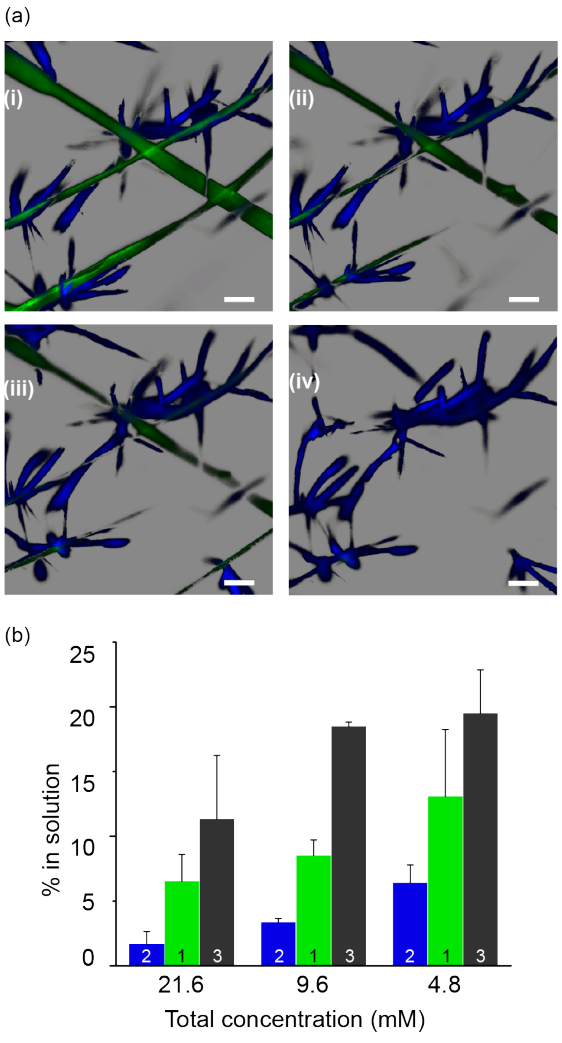

Figure 2: Solubility differences allow for selective supramolecular template removal. (a) Confocal microscopy time-lapse images showing selective removal of green scaffold (**1**) by slow addition of sodium dithionite DT while keeping the blue fluorescent assemblies of **2** intact. Scale bars: 50 µm, time interval between images i–iv: 20 min. **(b)** Percentage of soluble molecules as a function of total solution concentration of individual assemblies of **1**–**3**, determined by ^{1}H NMR in comparison with a soluble internal standard (hydroquinone).

It is not entirely fair to make such simple assumptions based on chemical reactivity considering electron donating groups. In fact, when measuring the conversion rates of **1'→1** and **2'→2** we are starting from completely homogenous and monomeric hydroxysulfonates that react with HCHO. When viewing the conversion of **1→1'** and **2→2'**, we start in the assembled state with micrometer-sized structures. It takes time for the DT to penetrate and react with structures of these sizes. However, DT can react more quickly with species that are in their monomeric state. NMR studies showed a higher proportion of soluble molecules for **1** than **2** (Figure 2b), due to their solubilizing hydroxyl groups. We therefore think that DT reacts preferentially with soluble **1** molecules, and therefore induces the selective depolymerization of **1** fibers, as we have observed experimentally. That is, a depletion of **1** monomers below the critical aggregation concentration, causes **1** molecules to be extracted from **1** fibers. In effect, **1** fibers act a removable supramolecular template for the growth of **2** structures. We could confirm the latter hypothesis using NMR by treating chemically fueled assemblies of **1** with different DT concentrations. DT when below the net concentration of HCHO+**1** (soluble monomers**)** did not lead to **1'**, and was preferentially consumed by excess HCHO. At concentrations comparable to HCHO+**1**(soluble monomers**)** we could observe quick conversion of soluble **1** monomers to **1'**. Once the DT was consumed, we observed monomers of **1** reappearing in the solution along with **1'** due to dissolution of the aggregates. At much higher concentration of DT all the molecules of **1** (soluble+aggregates) were quickly converted to **1'** (SI section 3.7, SI Figure S8).

Mechanical properties of multi-component gels

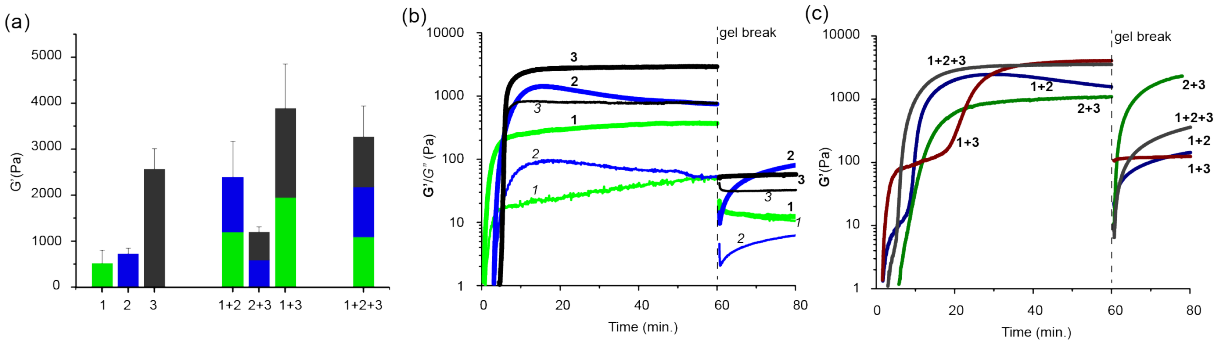

Figure 3: Mechanical characterization of chemically fueled multicomponent gels. (a) Storage moduli (G') of one, two, and three component chemically-fueled self-sorted hydrogels. **(b)** Time-evolution of hydrogels after adding HCHO to hydroxysulfonate **1'**, **2'**, or **3'** solutions. Gel breaking (dashed vertical line) was performed by applying a high shear rate (1000 s^{-1}) at 60 min. **(c)** The same as panel **b** but for two, and three component mixtures.

The mechanical properties of single and multicomponent self-sorted hydrogels were evaluated by rheology (Figure 3, see triplicate runs in Figure S6). To this end, solutions of **1'**, **2'**, or **3'** or mixtures of the latter three always at a total concentration of 35 mM, were quickly mixed with an excess of HCHO and placed between the parallel plates of the rheometer (see Section 3.8 of the SI). Compound **1** formed unstable hydrogels that expelled solvent under slight perturbation (ca. 500 Pa, see Figure 3a) probably because its rigid crystalline fibers could not percolate solvent properly. Hydrogels of **2** evolved quickly to reach a high *G'* (ca. 2000 Pa) but eventually stabilized to lower values (ca. 700 Pa). The latter can be seen in Figure 3b, where a maximum in *G'* and *G"* was reached around 17 minutes, after which both decrease and reach a plateau. This behavior can be due to quick formation of numerous small assemblies (see SI Figure S2a), but in the longer run, absence of long fibers would results in partial sedimentation of the assemblies to give the final *G'* values. Hydrogels of **3** had the best mechanical response (see black bar in Figure 3a and black lines in panel b), forming the stiffest of the three materials due to their long wavy fibers that are typically seen in supramolecular hydrogels. Interestingly, hydrogels consisting of **1**+**2** structures—formed by secondary nucleation of **2** on **1**—had significantly higher mechanical strength (ca. 2300 Pa) than either **1** or **2** alone (Figure 3a,c). In contrast, solvent expulsion (for **1** alone) or settling of

aggregates (for **2** alone) was not observed. Instead, the blue branches of **2** on fibers of **1**, seem to give rise to better entanglement and thus the formation of a more stable hydrogel. Another interesting feature, was the step-wise evolution of *G'* for **1**+**3** self-sorted gels (red line in Figure 3c). From microscopy we know that **1** forms first, followed by **3** that is the slowest to nucleate (see Figure S3d and SI Movie 3). Interestingly, the total *G'* of **1**+**3** is ~50 % higher than that of **3** alone, at just half the concentration of **3**. The high mechanical strength can be attributed to the presence of long extended fiber networks from both the individual components where the second network fills in the empty spaces to create a more densely packed hydrogel. In contrast, the **2**+**3** combination formed hydrogels with a lower mechanical strength (1200 Pa) than pure **3**, but slightly above that of pure **2** (Figure 3a,c). The three component system (**1**/**2**/**3** in ratio 0.33/0.33/0.33) was comparable to **1**+**3** gels.

The ability of these gels to self-heal after applying a high shear rate (1000 s^{-1}) for 30 seconds was also evaluated. Hydrogels of **1**, once sheared, could not recover ($G' \approx G'' \approx$ 10 Pa) and separation of solvent from fibers was observed. Further, gels of **2** could only partially recover to about 10% of their initial *G'*. The long fibers of **3** somewhat resisted total disruption of the gel properties, but the self-healing only recovered ~ 4% of the initial *G'*. Similarly poor recovery after shear damage was observed for **1**+**2** and **1**+**2**+**3,** whereas **1**+**3** did not show any recovery. In sharp contrast, **2**+**3** could recover and form gels that were stronger even than the initial self-sorted **2**+**3** gels. Apparently, the **2**+**3** gel shows a synergistic interaction between fibers of **3** and spherulites of **2**. The latter synergy presents intriguing prospects for other multicomponent self-sorted gels and materials, which can have materials properties—such as self-healing—that are not observed in the respective single component materials.

3. Conclusions and outlook

We showed how chemical fuels can be used to construct multicomponent self-sorted hydrogels. Subtle differences in the chemical structure of the hydrogelators affected both their reactivity toward the chemical fuels, as well as their propensity to self-assemble. The result is that intricate self-sorted materials could be made of molecules that using traditional approaches (e.g., heat/cool) would form poorly ordered co-assemblies. Our approach even allows for supramolecular templates to be used. That is, a first assembly guides the second, after which the first can selectively remove.

Man-made chemically fueled systems have already shown fascinating properties such as oscillations,[26] dynamic vesicles,[27] and transient assemblies[21, 28, 29], but have not been applied to control the hierarchy of multicomponent systems. Although ATP-powered transiently self-sorted colloids have been shown using DNA building blocks,[30] a similar approach in chemically fueled synthetic materials was lacking. We believe chemically fueled self-sorting provides a new method to achieve complex functional materials consisting of programmed orthogonal networks.

Acknowledgements.

N.S. would like to acknowledge Marie Curie Individual fellowship EU project 890659-CYCLOTUBES for funding. A.L-A. would like to acknowledge European Union's Horizon 2020 research and innovation programme under the Marie Skłodowska-Curie grant agreement no. 812868 for PhD funding. G.J.M.F. received funding from Ministère de l'Éducation Nationale de l'Enseignement supérieur et de la Recherche. T.M.H would like to acknowledge funding from ERC-2017-STG "Life-Cycle" (757910). We would like to thank Cyril Antheaume for his help with all the NMR and mass experiments. N.S. and A.L-A. contributed equally to the work.

Received: ((will be filled in by the editorial staff))
Revised: ((will be filled in by the editorial staff))
Published online: ((will be filled in by the editorial staff

References:

1. Sun, Y.; Bentolila, L. A.; Deming, T. J., Self-Sorting Microscale Compartmentalized Block Copolypeptide Hydrogels. *ACS Macro Letters* **2019,** *8* (10), 1275-1279.
2. Chen, H.; Huang, C.; Deng, Y.; Sun, Q.; Zhang, Q.-L.; Zhu, B.-X.; Ni, X.-L., Solvent-Switched Schiff-Base Macrocycles: Self-Sorting and Self-Assembly-Dependent Unconventional Organic Particles. *ACS Nano* **2019,** *13* (3), 2840-2848.
3. He, H.; Zheng, H.; Ma, M.; Shi, Y.; Gao, Z.; Chen, S.; Wang, X., Chirality on dendrimers: "roll booster" of the molecule-level self-sorting assembly in two-component supramolecular gel system. *Chemical Communications* **2020,** *56* (20), 2983-2986.
4. Sahoo, J. K.; VandenBerg, M. A.; Ruiz Bello, E. E.; Nazareth, C. D.; Webber, M. J., Electrostatic-driven self-sorting and nanostructure speciation in self-assembling tetrapeptides. *Nanoscale* **2019,** *11* (35), 16534-16543.
5. Panja, S.; Dietrich, B.; Shebanova, O.; Smith, A. J.; Adams, D. J., Programming Gels Over a Wide pH Range Using Multicomponent Systems. *Angewandte Chemie International Edition* **2021,** *60* (18), 9973-9977.
6. Singh, N.; Maity, C.; Zhang, K.; Angulo-Pachón, C. A.; van Esch, J. H.; Eelkema, R.; Escuder, B., Synthesis of a Double-Network Supramolecular Hydrogel by Having One Network Catalyse the Formation of the Second. *Chemistry – A European Journal* **2017,** *23* (9), 2018-2021.
7. Smith, M. M.; Smith, D. K., Self-sorting multi-gelator gels—mixing and ageing effects in thermally addressable supramolecular soft nanomaterials. *Soft Matter* **2011,** *7* (10), 4856-4860.
8. Moffat, J. R.; Smith, D. K., Controlled self-sorting in the assembly of 'multi-gelator' gels. *Chemical Communications* **2009,** (3), 316-318.
9. Singh, N.; Zhang, K.; Angulo-Pachón, C. A.; Mendes, E.; van Esch, J. H.; Escuder, B., Tandem reactions in self-sorted catalytic molecular hydrogels. *Chemical Science* **2016,** *7* (8), 5568-5572.
10. Singh, N.; Escuder, B., Competition versus Cooperation in Catalytic Hydrogelators for anti-Selective Mannich Reaction. *Chemistry – A European Journal* **2017,** *23* (41), 9946-9951.
11. Draper, E. R.; Eden, E. G. B.; McDonald, T. O.; Adams, D. J., Spatially resolved multicomponent gels. *Nature Chemistry* **2015,** *7* (10), 848-852.
12. Draper, E. R.; Adams, D. J., Low-Molecular-Weight Gels: The State of the Art. *Chem* **2017,** *3* (3), 390-410.
13. Castilla, A. M.; Draper, E. R.; Nolan, M. C.; Brasnett, C.; Seddon, A.; Mears, L. L. E.; Cowieson, N.; Adams, D. J., Self-sorted Oligophenylvinylene and Perylene Bisimide Hydrogels. *Scientific Reports* **2017,** *7* (1), 8380.
14. Morris, K. L.; Chen, L.; Raeburn, J.; Sellick, O. R.; Cotanda, P.; Paul, A.; Griffiths, P. C.; King, S. M.; O'Reilly, R. K.; Serpell, L. C.; Adams, D. J., Chemically programmed self-sorting of gelator networks. *Nature Communications* **2013,** *4* (1), 1480.
15. Draper, E. R.; Lee, J. R.; Wallace, M.; Jäckel, F.; Cowan, A. J.; Adams, D. J., Self-sorted photoconductive xerogels. *Chemical Science* **2016,** *7* (10), 6499-6505.
16. Draper, E. R.; Dietrich, B.; Adams, D. J., Self-assembly, self-sorting, and electronic properties of a diketopyrrolopyrrole hydrogelator. *Chemical Communications* **2017,** *53* (11), 1864-1867.
17. Cross, E. R.; Sproules, S.; Schweins, R.; Draper, E. R.; Adams, D. J., Controlled Tuning of the Properties in Optoelectronic Self-Sorted Gels. *Journal of the American Chemical Society* **2018,** *140* (28), 8667-8670.
18. Piras, C. C.; Smith, D. K., Sequential Assembly of Mutually Interactive Supramolecular Hydrogels and Fabrication of Multi-Domain Materials. *Chemistry – A European Journal* **2019,** *25* (48), 11318-11326.
19. Okesola, B. O.; Wu, Y.; Derkus, B.; Gani, S.; Wu, D.; Knani, D.; Smith, D. K.; Adams, D. J.; Mata, A., Supramolecular Self-Assembly To Control Structural and Biological Properties of Multicomponent Hydrogels. *Chemistry of Materials* **2019,** *31* (19), 7883-7897.

20. Wang, Y.; Lovrak, M.; Liu, Q.; Maity, C.; le Sage, V. A. A.; Guo, X.; Eelkema, R.; van Esch, J. H.; Hierarchically Compartmentalized Supramolecular Gels through Multilevel Self-Sorting. *Journal of the American Chemical Society* **2019***, 149*, 2847-2851.
21. Singh, N.; Lainer, B.; Formon, G. J. M.; De Piccoli, S.; Hermans, T. M., Re-programming Hydrogel Properties Using a Fuel-Driven Reaction Cycle. *Journal of the American Chemical Society* **2020,** *142* (9), 4083-4087.
22. Hammett, L. P., The Effect of Structure upon the Reactions of Organic Compounds. Benzene Derivatives. *Journal of the American Chemical Society* **1937,** *59* (1), 96-103.
23. Pinchas, S., Intramolecular hydrogen bonding in o-nitrobenzaldehyde and related compounds. *The Journal of Physical Chemistry* **1963,** *67* (9), 1862-1865.
24. Jezierska-Mazzarello, A.; Szatyłowicz H Fau - Krygowski, T. M.; Krygowski, T. M., Interference of H-bonding and substituent effects in nitro- and hydroxy-substituted salicylaldehydes. *Journal of Molecular Modeling* **2012,** *18* (0948-5023), 127-135.
25. Lampert, H.; Mikenda, W.; Karpfen, A., Intramolecular Hydrogen Bonding in 2-Hydroxybenzoyl Compounds: Infrared Spectra and Quantum Chemical Calculations. *The Journal of Physical Chemistry* **1996,** *100* (18), 7418-7425.
26. Leira-Iglesias, J.; Tassoni, A.; Adachi, T.; Stich, M.; Hermans, T. M., Oscillations, travelling fronts and patterns in a supramolecular system. *Nature Nanotechnology* **2018,** *13* (11), 1021-1027.
27. Wanzke, C.; Jussupow, A.; Kohler, F.; Dietz, H.; Kaila, V. R. I.; Boekhoven, J., Dynamic Vesicles Formed By Dissipative Self-Assembly. *ChemSystemsChem* **2020,** *2* (1), e1900044.
28. Boekhoven, J.; Hendriksen, W. E.; Koper, G. J. M.; Eelkema, R.; van Esch, J. H., Transient assembly of active materials fueled by a chemical reaction. *Science* **2015,** *349* (6252), 1075.
29. Singh, N.; Formon, G. J. M.; De Piccoli, S.; Hermans, T. M., Devising Synthetic Reaction Cycles for Dissipative Nonequilibrium Self-Assembly. *Advanced Materials* **2020,** *32* (20), 1906834.
30. Deng, J.; Walther, A., ATP-powered molecular recognition to engineer transient multivalency and self-sorting 4D hierarchical systems. *Nature Communications* **2020,** *11* (1), 3658.31.
31. Hansen, P. E.; Kamounah, F. S.; Saeed, B. A.; MacLachlan, M. J.; Spanget-Larsen, J., Intramolecular Hydrogen Bonds in Normal and Sterically Compressed o-Hydroxy Aromatic Aldehydes. Isotope Effects on Chemical Shifts and Hydrogen Bond Strength. *Molecules* **2019**, 24 (24), 4533.